UABeam: UAV-Based Beamforming System Analysis with In-Field Air-to-Ground Channels

Yan Shi, Rita Enami, John Wensowitch, and Joseph Camp
Department of Electrical Engineering, Southern Methodist University

***Abstract*— Precise air-to-ground propagation modeling is imperative for many unmanned aerial vehicle (UAV) applications such as search and rescue, reconnaissance, and disaster recovery. Furthermore, directionalization via MIMO-based beamforming can boost the transmission range by utilizing Channel State Information (CSI). However, the high mobility and flight conditions of drones can threaten the ability to receive accurate CSI in time to achieve such gains. In this work, we design a UAV-based software defined radio (SDR) platform and perform a measurement study to characterize the air-to-ground channel between the aerial platforms and a terrestrial user in practical scenarios such as hovering, encircling, and linear topologies. Our experiments cover multiple carrier frequencies, including cellular (900 MHz and 1800 MHz) and WiFi (5 GHz) bands. Furthermore, we address three baseline issues for deploying drone-based beamforming systems: channel reciprocity, feedback overhead, and update rate for channel estimation. Numerical results show that explicit CSI feedback can increase throughput by 123.9% over implicit feedback and the optimal update rate are similar across frequencies, underscoring the importance of drone-based beamfoming design. We additionally analyze the reciprocity error and find that the amplitude error remained steady while the phase error depends on mobility. Since our study spans many critical frequency bands, these results serve as a fundamental step towards understanding drone-based beamforming systems.**

***Index Terms*—Air-to-ground Channels, UAVs, Drones, Beamforming, Multiple Bands, Channel Estimation**

I. Introduction

Commercial drones are taking the world by storm - the global market for drones is expected to reach $22.15 billion by 2022 [1]. Recently, the deployment of low altitude platforms (LAPs) or UAVs has enabled wireless communication for ground-based terminals in applications such as disaster relief systems, public safety, and military communications. Drones can play a significant role in search and rescue operations, communication system recovery, and damage assessment for natural disasters like earthquakes, volcanoes, floods, or wildfires [2], due to rapid deployment and access to "hard-to-reach" geographic regions such as rivers, mountains and forests. In the public safety sector, UAVs have delivered broadband data rates in emergency and public safety situations, such as law enforcement and fire rescue [3]. Another emerging application is military communications where the role of drones has expanded from conventional missions like surveillance and reconnaissance to special forces for such applications as electronic interference, node swarms, and long-haul communication relays, each of which has traditionally relied upon soldiers or terrestrial-based vehicles [4], [5].

The future development of airborne wireless communication necessitates precise channel characterization and system-level performance analysis due to increasing deployments of aerial communication systems and their resulting data services. Theoretical studies that have characterized air-to-ground radio propagation for aircrafts have been widely conducted but mainly limited to simulation works that lack experimental validation [6]–[10]. Although these works have simulated air-to-ground channels in urban environments, most of the aforementioned works lack in-field data with real geographical features, which are crucial to drone-based applications.

While one work conducted in-field experiments with 970 MHz and 5.6 GHz with a single antenna, none of these works housed a software defined radio (SDR) platform on a drone to implement and evaluate beamforming techniques, which are gaining ever-increasing relevance for future generations of wireless networks. Beamforming plays a significant role in the spectral efficiency and data transmission in wireless systems, especially for orthogonal frequency division (OFDM) systems, which have been successfully implemented in widely-deployed wireless infrastructures, including IEEE 802.11 wireless LAN standards (WiFi), IEEE 802.16 Wireless MAN standard (WiMax), and 3GPP Long-Term Evolution (LTE). Many works have studied the benefits of beamforming [12], but the vast majority of these works focus on terrestrial networks which are not completely applicable to practical drone-based networks. For example, the cellular tower will always be fixed in location and lack the vibrations of a hovering drone. Lastly, many works assume ideal channel knowledge or error-free, instantaneous feedback [13], motivating the need for an in-field analysis of air-to-ground channel characterization and feedback analysis for UAV-based beamforming systems.

In this work, we design a prototyping testbed, UABeam, which implements drone-based beamforming using a USRP-based SDR platform (a battery-powered 2×2 MIMO Ettus E312) mounted via 3D printing to a DJI Matrice 100 drone. We develop an IEEE 802.11-based mechanism to support the channel feedback required for beamforming. Then, we conduct variable-range propagation experiments and characterize air-to-ground links as a function of distance, frequency, and drone altitude by analyzing the dominant propagation parameters (*e.g.*, the path loss and shadowing) on a wide range of frequency bands. We additionally evaluate the system-level performance of beamforming in terms of Bit Error Rate (BER) and throughput with in-field measurements. To evaluate the channel feedback required for drone-based beamforming gains, we use the three distinct scenarios of hovering, encircling, and linear: (*i.*) in the hovering case, the drone is hovering at a fixed altitude and location, (*ii.*) in the encircling case, the drone moves at a steady speed around a circle with the user equipment (UE) in the center, and, (*iii.*) in the linear case, the drone is passing by the ground receiver in a straight line.

The main contributions of this paper are as follows:

- We propose UABeam, the first prototyping system on drones that realizes air-to-ground communication using

978-1-5386-4281-8/18/$31.00 ©2018 IEEE

beamforming techniques across three commonly-used frequency bands (900 MHz, 1800 MHz, and 5 GHz).
- We implement UABeam on a USRP-based SDR platform by developing a physical (PHY) and media access control (MAC) design that allows explicit feedback for beamforming using IEEE 802.11-like signaling.
- We propose a relay-based feedback approach that expedites CSI feedback and saves computation cost at the receiver compared to existing feedback approaches.
- We conduct experiments within a repeatable variable-range scenario to characterize the air-to-ground channel and link performance of airborne beamforming, showing significant performance improvement over the conventional IEEE 802.11 scheme as a baseline for comparison.
- We evaluate channel reciprocity with three in-the-field scenarios to compare explicit and implicit feedback for drone-based beamforming, demonstrating that implicit feedback can largely degrade system performance.
- We investigate the optimal update rate for channel estimation in airborne communications and find that the optimal rate is mostly independent of carrier frequency.

The rest of this paper is organized as follows. We introduce the system model of UABeamin Section II. In Section III, we discuss the experimental setup and procedure. We conduct variable-range link experiments in Section IV. We evaluate channel feedback with hovering and encircling scenarios in Section V and a linear scenario in Section VI. Finally, we discuss related work in Section VII and conclude in Section VIII.

II. UABeam System and Feedback Analysis

In this section, we discuss the challenges that beamforming presents to UAVs, the 802.11-based signaling mechanism that allows CSI feedback in our UABeam system, and quantify the feedback overhead that exists in such a system.

A. Challenges of Drone-Based Beamforming

Beamforming systems are particularly suitable for air-to-ground wireless communications due to the following abilities: (*i.*) combating high levels of channel fluctuations introduced by hovering and flying the aircraft, (*ii.*) overcoming the limited range of omni-directional antenna patterns, and (*iii.*) leveraging spatial diversity to improve wireless transmissions [14]–[16]. The performance of beamforming can be further enhanced in terms of BER and throughput if CSI is obtained in a timely and efficient manner, assuming multiple antennas can be mounted and sufficiently spaced at the transmitter. However, there are three major uncertainties to evaluate when it comes to deploying beamforming systems on a UAV. First, will the overhead induced by feeding back the CSI consume any beamforming gain, especially in highly mobile scenarios common to drones? Second, can channel reciprocity be assumed or exploited in some capacity to minimize feedback overhead? Third, how frequently does CSI have to be fed back to the transmitter to support various drone topologies and mobility patterns and what relationship does this update rate have with the carrier frequency? To address these uncertainties, we first analytically evaluate the feedback overhead before we experimentally investigate it in Sections V and VI.

We implement a completely real-time OFDM beamforming system with flow control, synchronization, signal processing, and performance analysis functionalities by means of GNU Radio. Consider a typical beamforming system with M transmit antennas, one single receive antenna, and K subcarriers. At the kth subcarrier, the same copies of signal symbol $s(k)$ ($E\left[|s|^2\right] = 1$) is coded by the beamformer prior to being sent to the UE from the mth transmit antenna. For the purpose of eliminating inter-symbol interference (ISI) introduced by frequency-selective multipath channel, the cyclic prefix (CP) is added at each OFDM symbol. We represent $h_m(k)$ as the complex channel information obtained in the path from the mth transmit antenna to the single receive antenna at the kth subcarrier. The length of one OFDM data frame is assumed to contain a fixed number of L OFDM symbols. The preamble has two OFDM symbols with known training data. Therefore, the received symbol at the kth subcarrier and lth OFDM symbol interval ($l = 1, ..., L$) can be written as:

$$r(k,l) = \sum_{m=1}^{M} h_m(k) w_m(k) s(k,l) + n(k,l) \tag{1}$$

Here, $w_m(k)$ represents the beamforming vector at the kth subcarrier, and $n(k,l)$ denotes the additive noise. Empirically, $h_m(k)$ can be assumed to be constant within one epoch (a brief period of message exchange consisting of training, feedback, and beamforming) and changes independently from other epochs with velocities less than 8 m/s when timely feedback schemes and proper packet lengths are configured [17]. A short packet length will lead to excessive header overhead and resulting low throughput, while a long packet length could cause relatively high BER due to outdated CSI. Hence, we experimentally examine these independence assumptions and the impact of the packet length for drone-based systems.

In this work, we choose conjugate beamforming at the beamformer due to its simplicity and efficiency [13]. However, the above beamforming model can also be applied with other beamforming techniques like Zero-Forcing or Singular Value Decomposition. The conjugate beamformer is given by:

$$w_m(k) = \frac{\tilde{h}_m(k)^*}{\|\tilde{h}_m(k)\|} \tag{2}$$

Here, $()^*$ is the conjugate transpose operation, and $\tilde{h}_m(k)$ is the estimated channel information based on training symbols.

B. IEEE 802.11 Frame Structure

We use the IEEE 802.11 PHY frame as the frame structure in this work, as shown in Fig. 1. One frame is composed of a preamble, a header symbol, and OFDM-based data symbols of payload length L. The preamble consists of short training sequences (STS) and long training sequences (LTS). Both the STS and LTS have the duration of two training OFDM symbols, and the header has a duration of one OFDM symbol.

Fig. 1. IEEE 802.11 PHY frame Structure

In the conventional IEEE 802.11 standard, a CTS packet is required when the receiver successfully decodes an RTS packet. In this work, RTS and CTS frames are assumed to have zero-sized data payloads. The preamble serves two purposes:

synchronization and channel estimation. The receiver detects the existence of a frame based on the correlation of the received stream with the known information in the time domain. The preamble of the RTS sent by the transmitter is also used for channel estimation in the frequency domain.

C. Feedback Overhead

In order to efficiently achieve beamforming, the receiver broadcasts back its estimate of CSI to the transmitter via the time division duplex (TDD) schedule. Considering aerial communication, one challenge is trying to expedite the feedback procedure at minimal loss, since a large feedback overhead will greatly degrade the throughput rate. However, existing works that have attempted to optimize the CSI feedback have not directly addressed air-to-ground situations [18]–[23]. A previously proposed criterion is used to determine the matrix in this precoder codebook out of which to choose. By means of Grassmannian subspace packing, [18] proposed an efficient method to determine the optimal codebook. In [19], the OFDM subcarriers are divided into clusters, and only the Karcher mean vector is used. [20] allows feedback compression with fewer bits for MIMO systems. However in these works, the receiver still needs to process the CSI and prepare the feedback with extra computational cost.

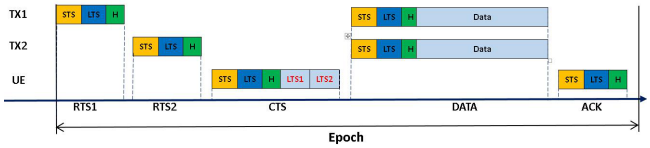

Fig. 2. Timeline of CSI Feedback for proposed beamforming scheme.

The MAC layer operation of our proposed CSI feedback method is shown in Fig. 2. In each epoch, CSI information is "relayed" to the transmitter by fully eliminating CSI processing at the receiver, which greatly expedites the feedback as well as limits power consumption. In particular, the transmitting antenna takes turns sending M RTS training messages to the receiver. Instead of performing CSI estimation on these received messages, the receiver directly attaches the received LTS to the end of the CTS feedback message to be sent. Note that the CTS contains $M+1$ LTSs, including M LTSs processed in the downlink direction, and one original LTS in the preamble. When the receiver sends back the CTS, all the LTSs are then processed by the uplink path. Assuming one training symbol from the LTS at the kth subcarrier is denoted as s_t, then the received symbols for M LTSs are given by:

$$r(s_t) = \overline{h}_m h_m s_t \tag{3}$$

The received symbol for the preamble LTS is given by:

$$\overline{r}(s_t) = \overline{h}_m s_t \tag{4}$$

where $\overline{h}_m$ is the uplink channel gain. Then, it is straightforward to obtain the downlink CSI by dividing $r(s_t)$ by $\overline{r}(s_t)$. Then, the data symbols are precoded by the beamformer at the transmitter prior to being sent to the receiver.

We compare our proposed feedback method with three previously-discussed approaches via simulation: (*i.*) G-subspace Codebook Index [18], (*ii.*) K-means Clustering [19], and (*iii.*) Vector Quantization [20]. For the convenience of this evaluation, we assume the transmitter and receiver are perfectly synchronized. We also assume the CSI can be perfectly obtained at the receiver. Now, the problem becomes how to feed back the CSI to the transmitter. For practical channel relevance, we implement the IEEE 802.11 Channel Model B with 11 taps [21]. We also implement conjugate beamforming at the transmitter equipped with two antennas but vary the transmission power. We evaluate the BER of the different feedback approaches as a function of SNR sensed by the receiver. We use QPSK as the data constellation order and calculate the BER for each method.

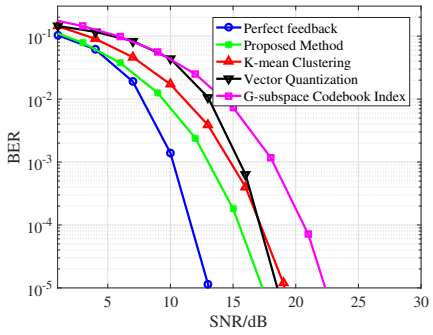

Fig. 3. BER Simulation under different feedback approaches.

Fig. 3 shows the simulation results of BER values for a 2×1 beamforming system employing our proposed approach, G-subspace Codebook Index, K-means Clustering, and Vector Quantization. Note that our proposed approach completely eliminates the feedback overhead at the receiver without sacrificing beamforming gain, while all other feedback schemes require various computational costs. A perfect feedback scenario is one where the receiver is assumed to feed back the CSI without any CSI loss with zero overhead cost. Our proposed approach has a BER improvement of 1.63 dB on average over that of K-means Clustering and 2.35 dB over that of Vector Quantization, respectively. At the low SNR, our proposed approach still provides the lowest BER of all four feedback schemes and comparable BER to perfect feedback. This can be explained by the channel quality having more impact on the conventional feedback schemes, which introduce extra feedback overhead and compression loss.

III. Hardware and Experimental Setup

To build UABeam for drone-based beamforming experimentation, we have designed and printed mounts for an Ettus E312 and two antennas to be secured on a DJI Matrice 100 (1-kg load capability), as shown in Fig. 4. To do so, we have used a ROBO 3D printer and CAD software to ensure that a 10-cm separation exists between two antennas for diversity purposes and allows repeatability in testing to position them in the same location. For a given experiment with a carrier frequency of 900 MHz and 1800 MHz, we mount two dual-band VERT900 omni-directional antennas, and for a given experiment at 5 GHz, we mount two dual-band VERT2450 antennas. Both antenna types provide a gain of 3 dBi. We have designed and implemented PHY and MAC layers that carry out the IEEE 802.11-like channel feedback signaling discussed in the previous section (Section II) using GNU Radio [24]. The receiver configuration is matched for the USRP hardware, but is housed on a tripod at a height of 1 m above the ground. The received signals are amplified and down modulated to

baseband. The digital samples are processed by GNU Radio blocks running on a Linux-based laptop.

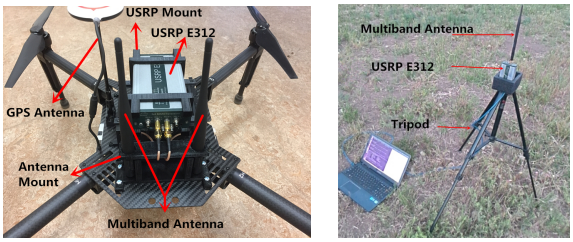

(a) (b)

Fig. 4. Equipment settings for experiments. (a) Beamformer USRP mounted on a drone (b) UE USRP mounted on a tripod.

TABLE I
IEEE 802.11 BASED FRAME PARAMETERS

Parameters	Preamble	Data
Modulation Schemes	BPSK	QPSK
Total Subcarriers	52	52
Occupied Subcarriers	52	48
Pilot Subcarriers	0	4
FFT size	64	64
CP Interval	0.25	0.25

Our experiments are conducted over three carrier frequencies: 900 MHz, 1800 MHz, and 5 GHz. At the PHY layer, we implement an OFDM scheme with 64 subcarriers operating with 20-MHz bandwidth, which is common for 802.11 systems. The preamble and header OFDM symbols use BPSK modulation but the data OFDM symbols use QPSK. The payload length is set to 256 bytes. At the MAC layer, we follow the periodic timeline schedule described in Fig. 2. We measure both BER and throughput to evaluate the beamforming system performance in the transmission environment. While many works use the Shannon Capacity to map the SNR or BER to the ideal information rate [25], for a practical frame-based system, the throughput depends closely on the hand-shaking overheads and successful decoding of the received frames [17]. In this work, the throughput (Mbps) is defined as the number of payload bits successfully recovered from the successfully decoded packets over the transmission time.

We conduct two different sets of experiments in the field. In the first set, we design experiments to evaluate the propagation and link performance at various transmitter-receiver separation distances, ranging from 10 to 100 m with 10-m granularity, and different drone hovering altitudes, ranging from 10 to 30 m with 10-m granularity. At each measurement position, the recording lasted 15 s, collecting 20M samples/s for each of the three carrier frequencies and in the 2 $\times$ 1 beamforming configuration. After the signal processing occurs, the received signal strength (RSS), BER, number of successfully decoded packets, and transmission period are extracted and then exported into a comma-separated format for post-processing.

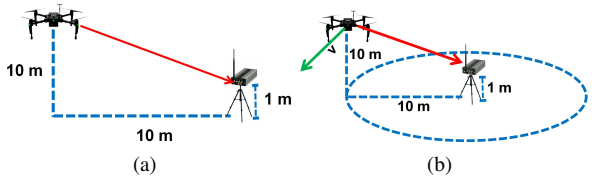

(a) (b)

Fig. 5. Channel Feedback Evaluation Topologies: (a) Hovering (b) Encircling

In the second set of in-field experiments, we first evaluate channel feedback approaches with both hovering and encircling scenarios to address the issues of channel reciprocity and update rate for channel estimation, as shown in Fig. 5. During our experiments, the average daily wind speed is reported to be approximate 5.7 m/s. In the hovering case, the drone maintains a height of 10 m and has a horizontal distance of 10 m from the receiver on the ground. In the encircling case, the drone follows a circular pattern at a horizontal radius of 10 m from the ground node in the middle of the circle with velocities reaching 6 m/s (this is full throttle in GPS mode due to the 500-g payload). To account for representative drone-based applications, we further evaluate the linear case, in which the drone is flying in a straight line approaching and leaving the ground node location. Additional details for the latter scenario can be found in Section VI.

IV. In-Field Link Analysis with Variable-Range Hovering Experiments

In this section, we perform in-field measurements to characterize the air-to-ground propagation channel and evaluate the link performance of beamforming. The transmitter and receiver have an unobstructed path as depicted in Fig. 6 with variable distances, carrier frequencies, and drone altitudes.

Fig. 6. Physical location of UABeam propagation experiments.

A. Baseline Path Loss Experiments: SISO Transmissions

For reference purposes, we first conduct SISO-based omni-directional experiments when the transmitter is on the ground (see Fig. 7(a) below) and hovering in the air (see Fig. 5(a)) at altitudes of 10 m, 20 m, and 30 m. With each transmitter location, the receiver is mounted on a tripod at a 1-m height at the specified ground-based distances from the transmitter's location. Based on the signal level at the receiver, we calculate the path loss exponent and shadowing component for each carrier frequency and transmitter altitude. The channel model from the transmitter to receiver can be described by the widely-used log-distance path loss model [29]–[31], given by:

$$P_{RX} = P_{TX} - PL_{d_0} - 10\gamma log_{10}(\frac{d}{d_0}) + X_s \qquad (5)$$

Here, PL_{d_0} is the path loss at a reference distance d_0, P_{RX} is the received signal strength, and P_{TX} is the transmission power. The term $10\gamma log_{10}(d/d_0)$ corresponds to the log-distance path loss, where d denotes the transmitter-receiver separation distance. Lastly, X_s is the shadow-fading parameter that follows a normal distribution with zero-mean and standard deviation σ. We use linear regression fitting to estimate the path loss exponent γ and the standard deviation σ.

We use a close-in (*e.g.*, 1 m) free-space reference distance to linearly fit the path loss (dB) as a function of distance (m) [17]. Assuming λ is the carrier wavelength, the path loss at the free space reference distance d_0 is given by:

$$PL_{d_0} = 20log_{10}(\frac{4\pi d_0}{\lambda}) \qquad (6)$$

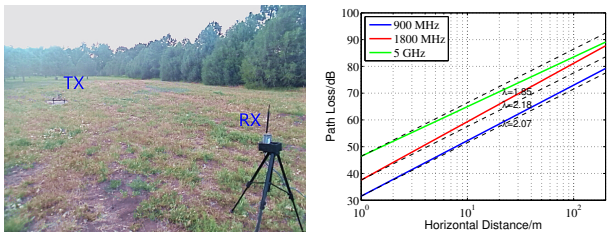

(a) (b)

Fig. 7. Ground-Based Reference Measurements. (a) Setup (b) Path Loss

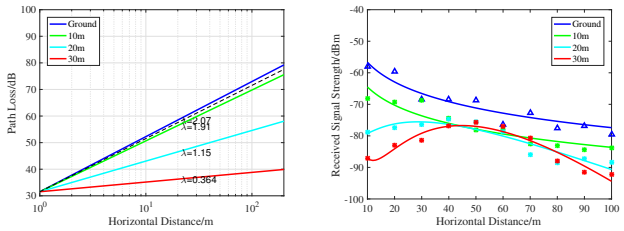

(a) (b)

Fig. 8. Variable-Range, Variable Altitude. (a) Path Loss (b) Signal Quality

Fig. 7(b) shows the path loss for the ground-based experiment after linearly fitting the measured values as a function of distance and frequency. We see that the 5-GHz path has the least path loss exponent of 1.85, which is less than free space. This can be explained by the existence of scatters that produce strong signal reflections in that frequency band. However, other frequency bands, such as 1800 MHz, show relatively larger path loss exponents.

Then, we repeat our experiments with different drone altitudes, ranging from 10 m to 30 m to investigate practical air-to-ground links influenced by the operation of drones. Fig. 8(a) presents the 900-MHz path loss behavior in the air-to-ground scenario. Surprisingly, the path loss exponents are far less than the expected free space value. Actually, this phenomenon happens in all of the frequency bands. Table II gives the estimated result of path loss exponent λ and shadowing standard deviation σ for each frequency band.

TABLE II
ESTIMATED LOG-DISTANCE PATH LOSS MODEL PARAMETERS

Parameter (Altitude)	900 MHz	1800 MHz	5 GHz
γ(10 m)	1.91	1.99	0.68
γ(20 m)	1.15	1.7	0.45
γ(30 m)	0.364	1.59	0.07
σ (10 m)	4.47	3.56	1.30
σ (20 m)	5.34	4.13	2.21
σ (30 m)	6.12	5.25	2.34

To dive deeper on why this odd phenomenon is occurring, Fig. 8(b) shows the 900-MHz band propagation results of the signal reception with the measurement data and resulting curve fit depicted as the solid lines. The signal reception based on the measurement position seem to follow the expected pattern when the drone is on the ground and at 10-m altitude: the received signal strength decreases as the distance increases. However, a curious pattern emerges at the higher altitudes: the received signal strength increases with distance at the shorter distances, and then decreases from the maximum value at greater distances. For example, 900 MHz has a peak value of -78 dBm at the distance of 50 m when the drone altitude is 30 m, and then the RSS value decreases when the distance increases, as you would expect from the log-distance path loss model. A similar effect occurs for 1800 MHz and 5 GHz. The reason is that the metal body of the drone is blocking the transmission at higher altitude and shorter distances. As the distance increases, the omni-directional transmission pattern is no longer blocked by the body. Additionally, Table II shows that the shadowing standard deviation increases as the altitude increases. In addition to the blocking problem already noted, the increase in shadowing at greater altitude could also be due to the increasing effect of the wind for the same weather conditions at increasing altitudes above the tree and building heights. In order to better describe the air-to-ground channel, we consider higher-order polynomials as shown in Fig. 8(b). The results at 20 m and 30 m of drone altitude are fit with a third-order polynomial function, creating a parabolic shape. However, the results at 10-m altitude still match a linear fit.

B. Beamforming-Based Link Performance Experiments

We now move to understanding the link performance of beamformed (2×1) transmissions that are housed on a drone at various heights (0-30 m) with a receiver at a 1-m height on a tripod and horizontal distances from 10-100 m. Fig. 9(a)(b)(c) and Fig. 9(d)(e)(f) present the BER and throughput, respectively, as a function of drone altitude, distance, and carrier frequency (900 MHz, 1800 MHz, and 5 GHz). Regarding BER, the two greatest altitudes (20 and 30 m) have a parabolic shape where the BER is initially reduced by increasing the distance and then increases with increased distance. This has a parallel to the SISO-based path loss experiments presented in the previous subsection, where the body of the UAV appears to be a blocking the signal at high altitude and short distances. Another interesting observation can be seen in Fig. 9(c), where there is a sizable difference in BER between the lower and higher altitudes as the distance increases. Unlike 900 and 1800 MHz, the hypotenuse of the triangle that forms between the altitude and the horizontal distance from sender to receiver is substantial in the 5 GHz case and causes substantially more loss. Regarding throughput, the increased height of 10 m has advantages at the greatest distances over the ground across all carrier frequencies. However, the throughput decreases from the ground-based transmission in all other cases except the 20-m altitude for 900 MHz (Fig. 9(d)). In particular, the 10 m altitude provides higher throughput at beyond around 75 m horizontal distance for 900 MHz and 1800 MHz, and around 50 m at 5 GHz, with an average throughput improvement of 89.3%, 76.5%, and 21.1%, respectively.

To quantify the throughput improvement compared with the conventional IEEE 802.11 SISO scenario without beamforming, we plot the normalized throughput gain of beamforming versus the SISO case under different drone altitudes in Fig. 9(g)(h)(i). We observe that beamforming always produces gains over SISO for 900 MHz at distances from 10-100 m (Fig. 9(g)), with at most a 39% throughput improvement. As the carrier frequency increases, the beamforming gains are restricted to a shorter range for the highest altitude with 1800 MHz (Fig. 9(h)) and for all altitudes with 5 GHz (Fig. 9(i)). The most air-to-ground gains across each carrier frequency occurs at a hovering altitude of 10 m, where beamforming provides improvements of up to 31%, 29%, and 21%, respectively, from lowest to highest carrier frequency.

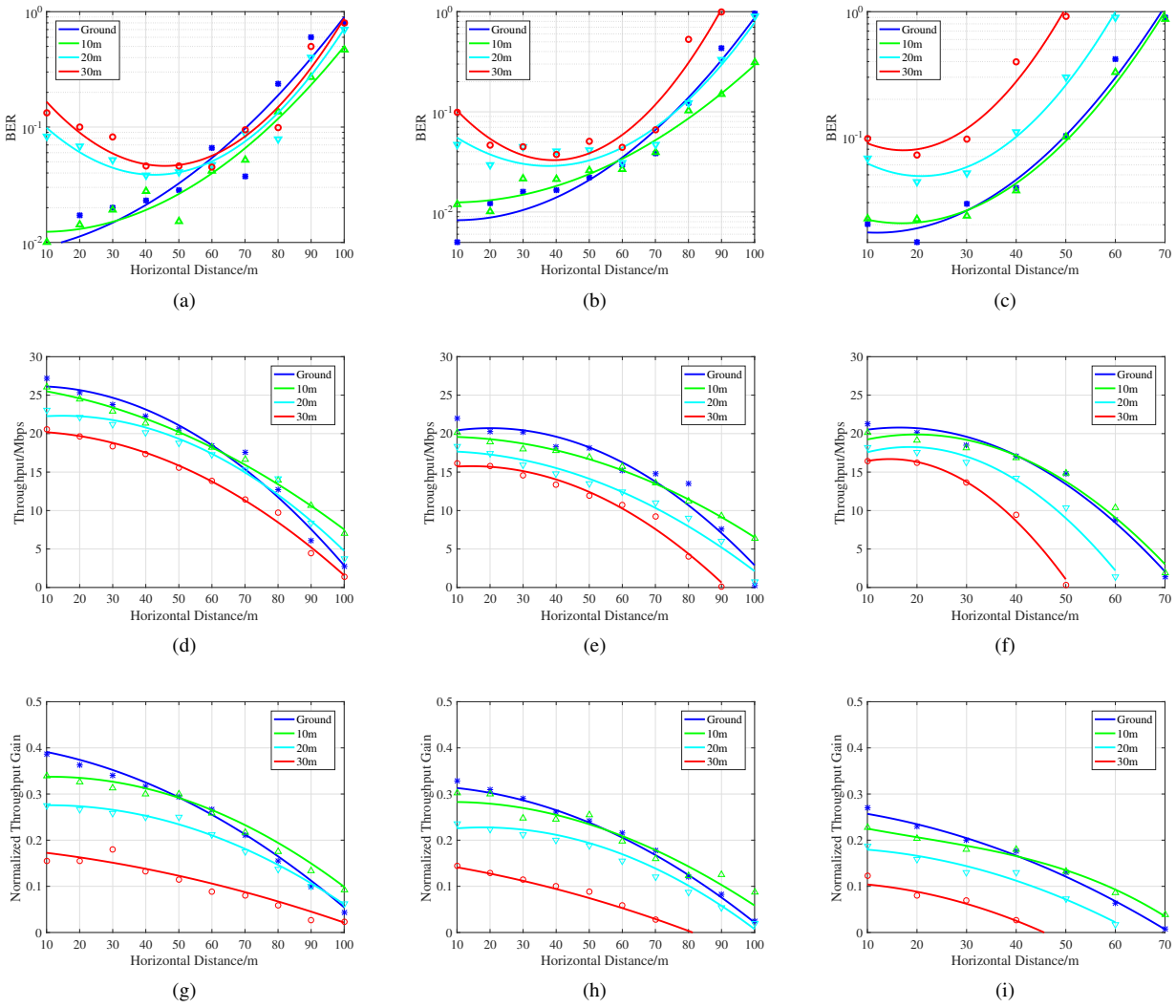

Fig. 9. BER vs. Distance plot of the air-to-ground channel: (a) 900 MHz (b) 1800 MHz (c) 5 GHz; Throughput vs. Distance plot of the air-to-ground channel: (d) 900 MHz (e) 1800 MHz (f) 5 GHz; Normalized Throughput Gain vs. Distance plot of the air-to-ground channel: (g) 900 MHz (h) 1800 MHz (i) 5 GHz.

V. In-Field Channel Feedback Evaluation with Hovering and Encircling Experiments

In this section, we use drone mobility to experimentally evaluate the specific issues of channel reciprocity and estimation update rate. The two forms of mobility include: (*i.*) a UABeam transmitter hovering in place and sending to a ground node and (*ii.*) a UABeam transmitter encircling a ground node with differing linear velocities (1 m/s, 3 m/s, and 6 m/s).

A. Channel Reciprocity

In the current IEEE 802.11 standard, two CSI feedback methods are defined: implicit feedback and explicit feedback. In both cases, CSI is estimated from the known training symbols in the preamble. For implicit feedback, the receiver sends the training symbols to the transmitter so that the transmitter can estimate the uplink channel. Since the downlink and uplink channels are assumed to be reciprocal, the transmitter implicitly obtains an estimate of the downlink channel by taking the transpose of uplink CSI. For explicit feedback, the transmitter first sends the training symbols to the receiver. After decoding the received signal, the receiver sends back the CSI to the transmitter. While explicit feedback can provide more accurate CSI, it introduces overhead in terms of time and feedback control bits.

The channel reciprocity assumption could be ill-suited for air-to-ground channels due to the severe mismatch in height of the communicating nodes and the susceptibility to severe channel fading with high levels of mobility. Therefore, we design baseline experiments using the UABeam system to explore and validate the performance of both feedback methods. To clearly demonstrate the effect of channel reciprocity, we first evaluate the relationship between the downlink and uplink channel information h_m and $\overline{h}_m$. Then, we investigate the throughput performance in both the hovering and encircling scenarios introduced in Section III. We capture the information mismatch between the uplink and downlink channel measured on consecutive forward and reverse traffic exchanges by defining the channel reciprocal error (CRE). The CRE at a specific subcarrier k is given by:

$$E_{cre} = \frac{h_m}{\overline{h}_m} \tag{7}$$

Previous works [27], [28] modeled the CRE as $E_{cre} = e_{env} \cdot e_{syn}$, where e_{env} denotes the propagation reciprocity error component contributed by hardware factors such as RF gain mismatch and antenna imperfections and environmental factors such as humidity, temperature, and altitude differences. e_{syn} denotes the reciprocity error component introduced by imperfect synchronization between the transmitter and receiver. The lack of synchronization stems primarily from the difference of arrival time between uplink and downlink channels (for TDD systems) and the frequency mismatch of the local oscillators, since OFDM signals are much more sensitive to frequency offsets [28]. The propagation reciprocity error can be expressed as:

$$e_{env} = A_{env} e^{j\theta_{env}} \tag{8}$$

Here, A_{env} and θ_{env} are modeled as normally-distributed and uniformly-distributed random variables, respectively. The synchronization reciprocity error e_{syn} can be expressed as:

$$e_{syn} = e^{j4\pi k\delta_p/N} \tag{9}$$

Here, δ_p is the the slope of the phase error denoted by the phase gradient, k is the subcarrier index, and N is the number of occupied subcarriers. Then, Eq. 7 is equivalent to:

$$E_{cre} = A_{env} e^{j(\theta_{env} + 4\pi k\delta_p/N)} \tag{10}$$

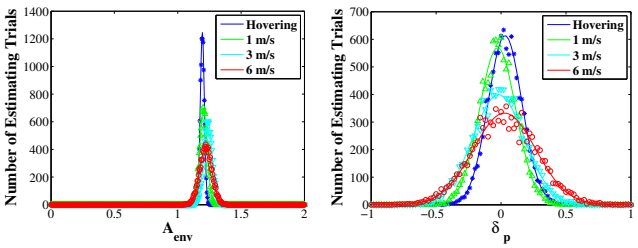

(a) (b)

Fig. 10. Distribution Analysis for CRE. (a) Amplitude (b) Phase Gradient

TABLE III
STATISTIC PARAMETERS OF CHANNEL RECIPROCITY ERROR RESULTS

Case	Frequencies	Mean(A_{env})	Std(A_{env})	Mean(δ_p)	Std(δ_p)
Hovering	900 MHz	1.19	0.016	0.031	0.13
	1800 MHz	1.06	0.029	-0.045	0.17
	5 GHz	0.85	0.038	-0.034	0.19
1 m/s	900 MHz	1.20	0.029	-0.026	0.14
	1800 MHz	1.07	0.033	-0.034	0.19
	5 GHz	0.85	0.039	-0.028	0.26
3 m/s	900 MHz	1.23	0.033	-0.019	0.20
	1800 MHz	1.10	0.036	0.028	0.25
	5 GHz	0.81	0.043	-0.026	0.26
6 m/s	900 MHz	1.22	0.048	0.027	0.24
	1800 MHz	1.16	0.057	-0.026	0.26
	5 GHz	0.79	0.059	0.016	0.29

During our experiments, the measured CRE results, such as amplitude error and phase error, are calculated as a function of the subcarrier obtained from every single sample measurement in both hovering or encircling experiments. The extraction of major parameters in the reciprocal error expression (10) are based on the minimum mean-square error (MMSE) criterion along obtained CRE results. Fig. 10 depicts a histogram in the form of four lines (superimposed to compare them) for each experiment for the different transmitting-drone velocities at 900 MHz. To form the histograms, the statistical distribution of parameters A_{env} and δ_p have bins of 0.005 and 0.02, respectively. These bins are extracted from 10000 channel samples for hovering and encircling experiments at 900 MHz. The solid line is a normally-distributed curve fit based on their mean and standard deviation. We found that A_{env} has a relatively narrow spike around an amplitude value. However, the width of various δ_p depends on the velocity of the drone, allowing either a positive or negative slope in the phase error. Similar results can also be found in other frequencies, as shown in Table III. Therefore, our analysis shows that while the amplitude error is approximately constant for both hovering and encircling experiments, the phase error for channel reciprocity highly depends on velocity.

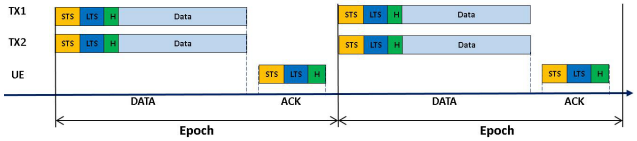

Fig. 11. Timeline of Implicit Feedback.

Beamforming systems will experience severe throughput degradation if imprecise channel feedback is obtained. As a result, we explore the impact of the reciprocity error on the throughput of the downlink conjugate beamforming system. We maintain the same experimental setup as before and have distinguished the downlink data transmissions with downlink CSI (explicit feedback) from the downlink data transmissions with uplink CSI (implicit feedback). Since implicit feedback does not necessarily require an RTS and CTS exchange, experiments with implicit feedback obtain CSI estimates based on the ACK message from the previous epoch, as shown in the timeline schedule in Fig. 11.

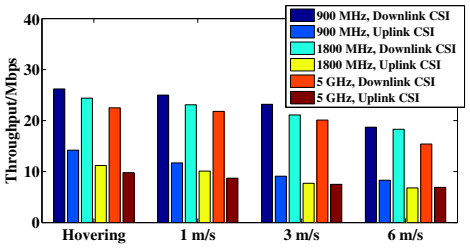

Fig. 12. Throughput results of beamforming system with channel reciprocity.

We have conducted an extensive set of experiments with the following traffic pattern: a packet payload of 256 bytes and average epoch interval of 200 ms over an experimental duration of 300 s. Fig. 12 shows the throughput results from a wireless experiment using downlink and uplink CSI for beamforming data transmissions at different frequencies and velocities. The beamforming throughput using explicit feedback (labeled Downlink CSI) can increase the throughput by 67.8%, 93.2%, and 103.9% over that using implicit feedback (labeled Uplink CSI) for 900 MHz, 1800 MHz, and 5 GHz in the hovering cases, respectively. The gains of explicit feedback are even greater when it comes to the encircling cases with a throughput improvement over implicit feedback of up to 92.6%, 111.6%, 123.9% for the aforementioned frequencies, respectively. We expect even greater throughput improvement for explicit feedback with higher velocities.

B. Update Rate for Channel Estimation

We investigate the update rate for airborne communications in terms of the number of OFDM symbols in a single data

frame, denoted by L. First, we explore the influence of the data length on the performance of BER and throughput for a given scenario and estimate the optimal length that leads to the maximum throughput for a given carrier frequency. This also corresponds to the optimal update rate for channel estimation. Second, we examine the optimal data length across different frequencies under the same experimental context.

We now test the hovering and encircling scenarios with the complete feedback signaling timeline shown in Fig. 3. As previously discussed, the downlink CSI is fed back using our proposed approach for every data frame, but the frame data length varies. We generate the packet source with the following packet lengths: $L \in \{32,64,128,256,512,1024,2048,4096\}$ and maintain the same transmission bandwidth. Note that 4096 is the maximum payload allowed in a single data frame according to the IEEE 802.11 standard.

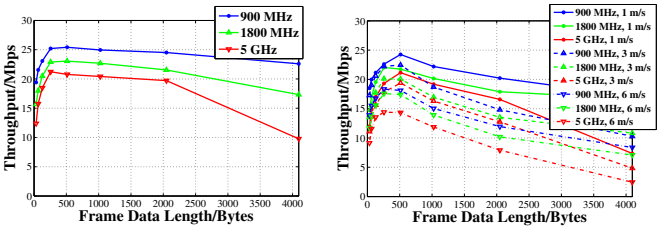

(a) (b)

Fig. 13. Throughput for various frame lengths: (a) Hovering (b) Encircling

The optimal packet length for the hovering scenario can be found in Fig. 13(a). For 900 MHz and 5 GHz the optimal rate is less than 512 bytes per data frame, while for 1800 MHz, the optimal rate is approximately 256 bytes per frame. In Fig. 13(b), the throughput decreases for the encircling scenario as drone velocity increases. However, the optimal update rates of 512 and 256 hold for their respective carrier frequencies regardless of the velocity. Based on these results, a reasonable universal packet size for UABeam communications would be 256 bytes across carrier frequencies.

VI. In-Field Instantaneous Performance Evaluation with Linear Experiments

In the previous section, we kept the physical distance constant between the transmitter and receiver in a hovering and encircling scenario to maintain a fixed average received power, but allow channel fluctuations according to the vibrations and mobility of a drone in flight. In this section, we consider the scenario where the drone is flying in a straight line from one edge of the range, coming closer to the ground station, and then on to the other edge of the range. The reason for doing this experiment is to introduce an additional variable beyond the channel fluctuations: a change in the average channel quality over the course of the experiment.

To do so, we design this linear experiment (see Fig. 14(a) below) where the drone maintains a height of 10 m, beginning at a distance of approximately 30 m from the ground station, progressing in a straight line toward the ground station, and ending at a distance of 30 m from the ground station. We then iterate over three different speeds (1 m/s, 3 m/s, and 6 m/s) and the aforementioned two different feedback mechanisms of explicit (labeled Downlink CSI) and implicit (labeled Uplink CSI). We seek to investigate the impact of channel reciprocity on beamforming performance when there is movement in the average channel quality coupled with the previously tested channel fluctuations. In other words, this scenario accounts for the comprehensive impact of channel fluctuation introduced by both changing velocities and ranges. We feel that the experiments now cover a wide range of scenarios that would be representative for various applications such as public safety, package delivery, and search and rescue. In these particular cases, the drone is rapidly approaching or moving away from the destination node while trying to maintain reliable communication links.

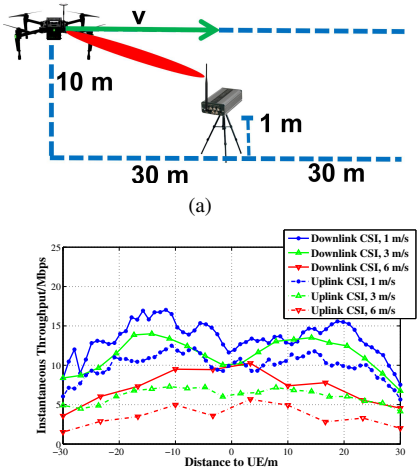

(a) (b)

Fig. 14. Instantaneous Throughput vs. Distance. (a) Setup (b) 900 MHz

Fig. 14(b) shows the in-field experimental results of instantaneous throughput for 900 MHz for the six iterations previously mentioned. The three velocities are indicated by different colors and markers of the same shape (blue circles for 1 m/s, green triangles pointing up for 3 m/s, and red triangles pointing down for 6 m/s). The solid lines represent the Downlink CSI, and the dotted lines represent the Uplink CSI. The relative distance is defined as the horizontal distance between drone and receiver UE. The instantaneous throughput is calculated over each 1 second window period of the experiment. The first observation is that compared to the hovering and encircling experiments (approximately 25 Mbps), the peak throughput values are lower for the linear topology (approximately 17 Mbps) even though the drone actually comes closer to the ground station. There are two factors contributing here: (i) the optimal beamforming weights are challenging to find even though the mobility is only 1 m/s and (ii) there is reduced received power directly below the drone (see Fig. 8). Second, we observe that explicit outperforms implicit feedback again in the linear topology with average throughput increases of 37.8%, 88.1%, and 105.1% for 1, 3, and 6 m/s, respectively. We see the greatest distinction occur at a relative distance of 17 m, which has a gain of 177.3% for explicit versus implicit.

VII. Related Work

Statistical models for predicting the air-to-ground path loss in urban environments have been proposed (*e.g.*, [6]). At the same time, simulation works have been performed to optimize the position of aircrafts to maximize the radio coverage in urban environments [7], [8]. A fading model that includes

rain attenuation, cloud attenuation, and gaseous absorption attenuation was proposed to characterize the realistic air-to-ground channel but only addressed High Altitude Platform (HAP) links [9]. System-level simulations also utilized path loss models to evaluate the performance of LTE and WiFi [10].

For in-field experimentation, the closest work to ours performed a measurement study of air-to-ground propagation at 970 MHz and 5.6 GHz with a single-antenna, omni-directional transmission pattern to characterize large-scale path loss modeling [11]. Various theoretical works focusing on beamforming techniques have been proposed to improve the performance (see [12] and references therein). Since the optimal beamformer obtained from eigen-decomposition that maximizes the average signal to noise ratio (SNR) along all UEs, there have been significant works concentrating on designing the optimal beamforming coding/decoding, improving the current channel estimation efficiency, and reducing the feadback payloads. However, most of these approaches focus on conventional ground-to-ground communication (common in Ad Hoc and WiFi scenarios) or tower-to-ground communication (common in cellular scenarios), which have severe limitations in their applicability to air-to-ground scenarios. For example, the tower will always be fixed in location and even lack the vibration of a hovering drone. In addition, current works either assume that both the receiver and transmitter have full channel knowledge or presume an ideal error-free feedback link [13]. However, both of these critical aspects cannot be ignored in any practical beamforming system. In contrast to these works and to the best of our knowledge, none of current published works perform in-field measurements on drone-based, air-to-ground communication over a wide range of critical frequency bands at transmitter distances typical for WiFi and cellular technologies.

VIII. Conclusion

In this work, we designed a system to evaluate propagation, link performance, and channel feedback mechanisms for drone-based beamforming in representative practical scenarios. To do so, we built a complete IEEE 802.11-like signaling mechanism across the MAC and PHY layers using a SDR platform. Then, we conducted in-field, variable-range hovering experiments to characterize the air-to-ground channel and link performance at various heights and distances. Next, we investigated implicit and explicit feedback with hovering, encircling, and linear experiments as well as reciprocity error evaluation. Our assessment covers a wide range of UAV communication bands, and numerical results demonstrate that a properly optimized drone-based beamforming system can provide significant throughput improvement using explicit versus implicit feedback. We believe these results will have far-reaching impact on the future design of real-world UAV MIMO communications.

ACKNOWLEDGMENTS

This work was in part supported by NSF grants: CNS-1150215 and CNS-1526269.

References

[1] "UAV Drones – Global Market Outlook (2016-2022)," *MRC*, 2016.
[2] M. Erdelj, E. Natalizio, K. R. Chowdhury, and I. F. Akyildi, "Help from the Sky: Leveraging UAVs for Disaster Management," *IEEE Pervasive Computing*, vol. 16, no. 1, 2017.
[3] E. Vattapparamban, . Gven, A. . Yurekli, K. Akkaya, and S. Uluaa, "Drones for smart cities: Issues in cybersecurity, privacy, and public safety," in *IEEE IWCMC*, 2016.
[4] D. Orfanus, E. P. de Freitas, and F. Eliassen,, "Self-Organization as a Supporting Paradigm for Military UAV Relay Networks," in *IEEE Commun. Lett.*, vol. 20, no. 4, 2016.
[5] M. Schulzke, "The Drone Revolution: The Morality of Drone Warfare and the Politics of Regulation," in *Palgrave Macmillan*, 2017.
[6] A. AlHourani, S. Kandeepan, and A. Jamalipour, "Modeling air-to-ground path loss for low altitude platforms in urban environments," in *IEEE GLOBECOM*, 2014.
[7] A. Al-Hourani, S. Kandeepan, and S. Lardner, "Optimal LAP altitude for maximum coverage," in *IEEE Wireless Commun. Lett.*, 2014.
[8] E. Kalantari, H. Yanikomeroglu, A. Yongacoglu, "On the Number and 3D Placement of Drone Base Stations in Wireless Cellular Networks," in *IEEE VTC*, 2016.
[9] Y. Zheng, Y. Wang, and F. Meng, "Modeling and Simulation of Pathloss and Fading for Air-Ground Link of HAPs within a Network Simulator," in *CyberC*, 2013.
[10] S. Chandrasekharan, A. Al-Hourani, K. Gomez, S. Kandeepan, R. Evans, L. Reynaud, and S. Scalise, "Performance Evaluation of LTE and WiFi Technologies in Aerial Networks," in *IEEE GLOBECOM*, 2016.
[11] D. W. Matolak and R. Sun, "Air-ground channel characterization for unmanned aircraft systems: The near-urban environment," in *IEEE MILCOM*, 2015.
[12] J. Mietzner, R. Schober, L. Lampe, W. H. Gerstacker and P. A. Hoeher, "Multiple-antenna techniques for wireless communications - a comprehensive literature survey," in *IEEE Communications Surveys & Tutorials*, vol. 11, no. 2, 2009.
[13] H. Yang and T. Marzetta, Performance of Conjugate and Zero-Forcing Beamforming in Large-Scale Antenna Systems, in *IEEE J. Sel. Areas Commun.*, vol. 31, no. 2, 2013.
[14] H. Jian, W. Yongsheng, and Z. Yuetong, "UAV communication channel estimation methods for OFDM system based on Akaike information criterion", *Journal of Circuits and Systems*, vol. 14, no. 1, 2009.
[15] Y. Zeng, R. Zhang, and T. J. Lim, "Wireless communications with unmanned aerial vehicles: opportunities and challenges," in *IEEE Commun. Mag.*, vol. 54, no. 5, 2016.
[16] Y. Shi, J. Wensowitch, E. Johnson, and J. Camp. "A Measurement Study of User-Induced Propagation Effects for UHF Frequency Bands," in *IEEE SECON*, 2017.
[17] A. Ghosh, J. Zhang, J. G. Andrews, and R. Muhamed, "Fundamentals of LTE," *Prentice Hall*, 2010.
[18] D. Love and R. W. Heath Jr., Limited feedback precoding for spatial multiplexing systems, in *IEEE GLOBECOM*, 2013
[19] T. Pande, D. J. Love, and J. V. Krogmeier, Reduced feedback MIMO-OFDM precoding and antenna selection, in *IEEE Trans. Signal Processing*, vol. 54, no. 5, 2007.
[20] Q. Wang, H. Feng, L. Cimini, L. Greenstein, D. Chan, and A. Hedayat, Comparison of quantization techniques for downlink multi-user MIMO channels with limited feedback, in *IEEE Wireless Commun. Lett.*, 2014.
[21] Joint Proposal Team PHY Simulation Results, IEEE 802.11r2, 2006.
[22] H. Zhang, Y. Li, V. Stolpman, and N. V. Waes, A reduced CSI feedback approach for precoded MIMO-OFDM systems, in *IEEE Trans. Wireless Commun.*, vol. 6, no. 1, 2007.
[23] Y. Ma, G. Zhou and S. Lin, "EliMO: Eliminating Channel Feedback from MIMO," in *2017 IEEE SMARTCOMP*, 2017.
[24] "The Main Page of GNU Radio," Available: https://wiki.gnuradio.org/index.php/Main_Page/
[25] Y. Du, E. Aryafar, P. Cui, J. Camp and M. Chiang, "SAMU: Design and implementation of selectivity-aware MU-MIMO for wideband WiFi," in *IEEE SECON*, 2015.
[26] Y. Shi and J. Camp, "Downlink Resource Allocation for Enhanced Inter-Cell Interference Coordination (eICIC) in Heterogeneous Cellular Networks," in *IJERSTE*, vol. 5, no. 2, 2016.
[27] Z. Gu, N. Wei, and Z. Zhang, "Analysis and modeling of channel reciprocity errors based on a experimental OFDM/TDD coordinated multipoint transmission system," in *IEEE ICCC*, 2013.
[28] M. Morelli, C. C. J. Kuo, and M. O. Pun, "Synchronization Techniques for Orthogonal Frequency Division Multiple Access (OFDMA): A Tutorial Review," in *Proceedings of the IEEE*, 2007.
[29] Y. Shi, "Improving the performance of RSS detection using wireless open-source platforms," in *IEEE Texas Symposium on WMCS*, 2015
[30] D. Xue, B. Garner, and Y. Li, "Investigation of short-range, broadband, on-body electromagnetic wave propagations", *IET Microwaves, Antennas & Propagation*, 2016.
[31] Y. Shi, R. Enami, J. Wensowitch, and J. Camp. "Measurement-Based Characterization of LOS and NLOS Drone-to-Ground Channels," in *IEEE WCNC*, 2018.